

Diffusion-controlled kinetics of carbon nanotube forest growth by chemical vapor deposition

Oleg A. Louchev, Thomas Laude, Yoichiro Sato, and Hisao Kanda
National Institute for Materials Science, 1-1 Namiki, Tsukuba, Ibaraki 305-0044, Japan

(Received 20 November 2002; accepted 29 January 2003)

A detailed theoretical study of carbon nanotube (NT) forest growth by chemical vapor deposition is given, including (i) ballistic mode of carbon species impingement into the NT surface, (ii) the carbon diffusion over NT surface and through the metal nanoparticle, and (iii) the temperature drop at the NT tip occurring with increase in NT length. For typical NT forest growth parameters the ballistic flux of carbon species impinging into the NT surface decays quasiexponentially within several microns from the top. A variety of feasible growth modes, ranging from linear to exponential versus time, is predicted agreeing well with reported experiments. The presence of a metal nanoparticle is shown to shift NT growth from being surface diffusion controlled to being controlled by bulk diffusion through the nanoparticle. For typical growth conditions the growth rate is shown to be controlled simultaneously by surface diffusion over NT surface and bulk diffusion of carbon through metal nanoparticle. However, even in specific cases where NT growth rate is controlled by bulk diffusion through the nanoparticle the initial stage may be controlled by surface diffusion, as revealed by the exponential change in NT length with time. A parametric study of the growth rate of NT forest with metal nanoparticles held at the NT tips as a function of temperature reveals the existence of a maximum near 1050–1100 K, agreeing with reported experimental data. A thermal analysis based upon the heat conductance equation shows that with NT forest growth the temperature of the NT tips decreases, leading to growth deceleration and termination. Our study shows that the larger the pressure the smaller the NT forest height that may be grown. In particular, for pressures $\approx 10^5$ Pa the NT tips should be “frozen” even at a length of a few microns, disabling further NT growth. In contrast, under low pressures of $\approx 10^3$ Pa NT forest of several dozens of microns may be successfully grown without significant growth deceleration. © 2003 American Institute of Physics. [DOI: 10.1063/1.1562195]

I. INTRODUCTION

The growth of well aligned C nanotube (NT) forests by chemical vapor deposition (CVD) or pyrolysis of hydrocarbons is an effective technique for NT production and has been studied by several groups trying to optimize the parameters of this process for cold electron emitters and other applications.^{1–28} Wherever the catalyst nanoparticles are found in growth experiments, i.e., on the NT tips or on the substrate, the majority of experimental reports^{1–27} refer to a model of carbon filament growth by continuous C diffusion or extrusion through the metal nanoparticle^{29–31} (“tip” or “base” growth model). However, NT forests have also successfully been grown by plasma enhanced CVD even without a catalyst,²⁸ suggesting that another kinetical mechanism may be involved in this process. Additionally, in our recent communication³² we have provided an order to magnitude analysis of CVD process of carbon NT forest growth outlining several contradictions which arise in the application of the model^{29–31} for a particular experimental study where the Fe catalyst remained at the bottom.¹⁸ We suggested another NT forest growth mechanism within the general framework of the surface diffusion (SD) model^{33–41} which may be responsible for CVD growth in many practically important cases.

In particular, the involvement of the SD mechanism

explains⁴¹ the existence of the exponential time dependence observed in NT growth.³⁰ In the case of open ended NT growth controlled by SD this exponential stage extends to the moment when the NT length reaches the length of surface diffusion, of the order 0.1–1 microns depending on T .⁴¹ However, experimental data related to the growth mediated by metal catalyst particles³⁰ shows that, when the particle is present, this exponential stage reduces to the order of 10 nanometers and even less, depending on the metal used. In our previous short communication on physical and chemical vapor deposition growth of NTs,^{32,39} we suggested that the metal nanoparticles do not play a significant role in feeding NT growth because the carbon flux is mainly provided by SD over the NT surface. In contrast, an early review³⁰ and other more recent papers, suggest that the growth is controlled by bulk diffusion through the metal particle.

In this paper we make an effort to resolve these, and other related issues by providing a comprehensive analysis based on an analytical model which includes both surface diffusion over NT surface and bulk diffusion of carbon through the metal particle. The resulting analytical expressions allow one to distinguish clearly various modes of forest growth and determine growth controlling effects under different growth conditions.

The paper is structured as follows: Section II focuses on

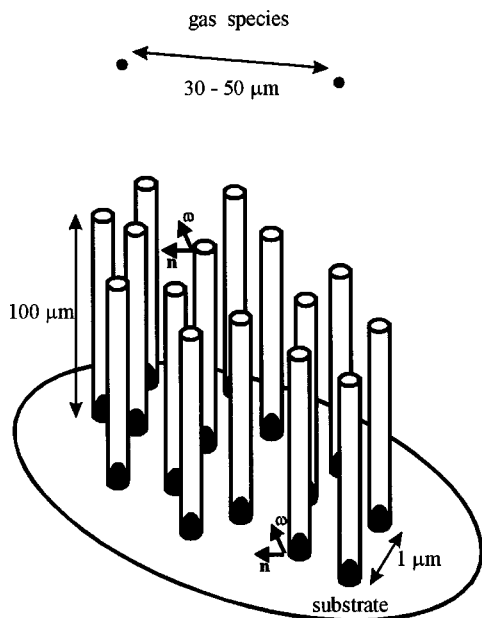


FIG. 1. Schematics of NT forest growth with metal particle NT bases.

analysis of the ballistic impingement rate of gas species along the NT surface. In Sec. III an analysis of possible effects caused by metal nanoparticles in NT formation is given. In this section we discuss also in detail the role of metal nanoparticles in the initial selection of NT growth modes, which defines whether the metal particle remains at the substrate or is held at the NT tip. In Sec. IV we discuss a transition from NT growth mode controlled by surface diffusion along the lateral surface of the NT to that controlled by the diffusion through the metal nanoparticle, both of which may take place depending upon the growth conditions. In this section we also investigate how the growth rate depends on the temperature, revealing the existence of the experimentally observed maximum. Section V is devoted to the study of thermal physics effects elucidating the mechanism of experimentally observed NT growth deceleration and termination. Section VI focuses on the main conclusions of our study.

II. BALLISTIC MASS TRANSFER IN NT FOREST

Let us consider parameters for a NT forest grown on a metal catalyst nanoparticle array (see Fig. 1) in order to analyze the transport phenomena in the gas phase involved in growth experiments.¹⁸ In this and many other practical cases where metal particles remain at the substrate, base growth via the diffusion of C through the particles cannot be involved in the latest postnucleation stages of NT forest growth, when the NT length exceeds several microns. This is because, to reach the metal nanoparticles remaining on the substrate, chemically active carbon species should penetrate through the forest. This looks to be impossible in view of the typical mean free path in the gas estimated as

$$l_g \approx k_B T / (\sqrt{2} \sigma P) \approx 30 - 50 \text{ } \mu\text{m}, \quad (1)$$

for operational conditions $P \approx 2600 \text{ Pa}$ ($\approx 20 \text{ Torr}$) and $T = 600 - 1000 \text{ K}$ (Ref. 18) ($\sigma \approx 10^{-19} \text{ m}^2$) which appears to be

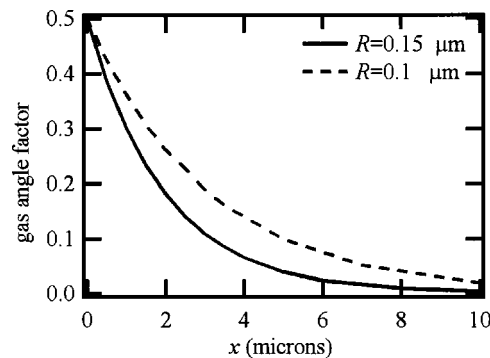


FIG. 2. Distribution of averaged angle factor along the NT surface from the top ($x=0$) to the bottom.

much higher than the intertube distance within the forest, $\approx 1/\sqrt{N} \approx 1 \text{ } \mu\text{m}$ (for NT surface density $N \approx 10^8 \text{ cm}^{-2}$). That is, inside the forest ballistic mass transfer takes place in which chemically active carbon species collide only with NTs without collisions with gas species, and therefore without diffusion along the intertube space to the forest bottom.

The ballistic penetration of species into the forest may be characterized by the distribution of the angle factor along the NT surface. This angle factor, which represents the ratio of impinging flux from the gas into a particular point of a NT surface shadowed by other NTs to the flux which would impinge into the surface from a hemispherical solid angle (unshadowed), is given by

$$F_{\text{gas}}(x, l) = \pi^{-1} \int_{\Omega} (\mathbf{w}, \mathbf{n}) d^2 \Omega, \quad (2)$$

where Ω is the solid angle within which the gas phase is "seen" from a particular point of the NT surface.

The distribution of the angle factor computed numerically and averaged over the NT circumference,

$$\bar{F}_{\text{gas}}(x) = \frac{1}{2\pi R} \int_0^{2\pi R} F_{\text{gas}}(x, l) dl \quad (3)$$

is given in Fig. 2 for the intertube separation $l_{\text{int}} = 1 \text{ } \mu\text{m}$ (Ref. 18) and for typical values of NT radius $R = 0.1 - 0.15 \text{ } \mu\text{m}$. It shows that the impingement rate decays rapidly towards the forest bottom. For a NT forest with NT radius $R = 0.1 \text{ } \mu\text{m}$ at a distance of $10 \text{ } \mu\text{m}$ from the top the impingement rate decreases by an order of magnitude (from 0.5 near the top to 0.02) and for $R = 0.15 \text{ } \mu\text{m}$ this decay is even more significant. These calculations show that the forest bottom may be reached only by a negligibly small amount of chemically active carbon species impinging within a small solid angle compared with solid angles on the NT top (see Fig. 1). The majority of species impinge into the NT surface within several microns of the top and do not penetrate to the bottom of a NT forest of several dozens of microns in depth.¹⁸ Let us note here that the distributions given in Fig. 2 may be well approximated by an exponential function, i.e., $0.5 \exp(-x/l^*)$ with characteristic decay length $l^* = 2 - 3 \text{ } \mu\text{m}$. For NT length $L \gg l_{\text{int}}$ we recommend an analytical

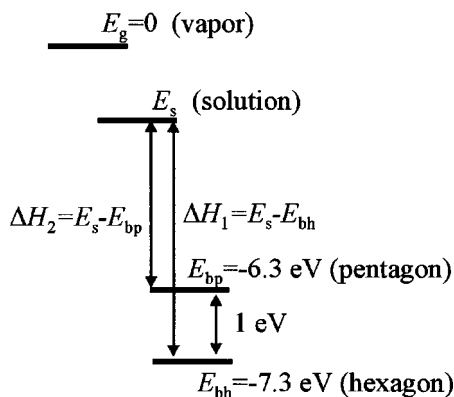


FIG. 3. Energy levels of carbon atoms in vapor, solution, and solid phase.

estimate for this parameter as $l^* \cong S/(\pi R)$, where S is area per one NT (estimated through NT surface density, N , as $S = 1/N$).⁴²

The NT surface represents a deep energy well for chemically active C species. For instance, a microenergetic study³⁴ gives ≈ 1.8 eV for the interaction of C atom (CH_3) with the NT surface. The values corresponding to chemisorption of carbon dimers (C_2H_2 radicals) should obviously be even higher due to twofold interaction with the NT surface. The contribution of CH_4 is negligibly small because of weak physical adsorption (Baker and Harris³⁰ reported on absence of carbon fiber growth from pure CH_4). Therefore, chemically active CH_3 and C_2H_2 units present in plasma or thermally excited gas^{43,44} should be captured by colliding with the NT surface within the top few microns, and are unable to penetrate to its bottom. It is also worth noting here that, assuming that NT growth occurs via C atom incorporation at the NT base on the substrate, an additional serious contradiction appears as to why the top part of NTs subject to significantly larger C fluxes remain uncovered by any kind of C deposit, i.e., graphite or amorphous carbon, which are known to appear in C film growth in hot filament or plasma assisted CVD using hydrocarbons. By contrast, assuming that NT growth occurs at the upper tip of the NTs and nonpenetration of chemically active carbon species to the forest bottom one can understand why the bottom part of the NT forest remains unfilled by any kind of carbon deposit, and why the bottom parts of NTs do not fatten with time.

III. THE ROLE PLAYED BY THE METAL NANOPARTICLE IN NT GROWTH

A. Bulk diffusion and surface diffusion effects

In nanotube growth metal nanoparticles play a very significant multifold role. For instance, metal nanoparticles act as nanoscale templates, enhancing NT nucleation by providing a near surface energy well⁴⁷ and predefine NT wall thickness.³¹ Metal nanoparticles are also shown to stabilize the growth of the NT wall against premature closure caused by pentagon formation on the growth edge.⁴¹ This effect is based on the fact that a C atom at a hexagon corner on the edge has significantly larger binding energy compared with that of an atom at the pentagon corner. This difference in

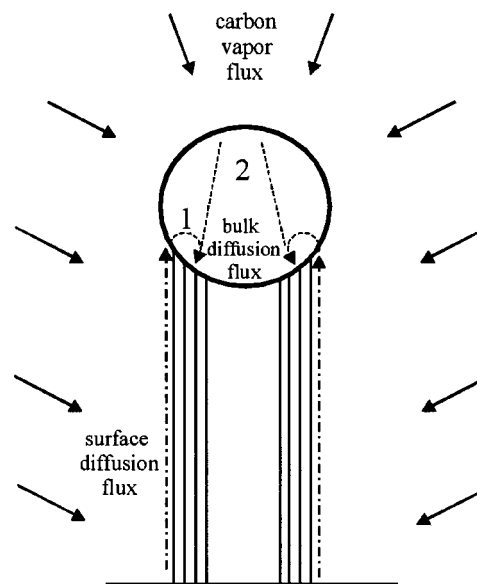


FIG. 4. Schematic of carbon pathways feeding NT growth via (i) impingement of carbon flux into the NT surface, surface diffusion over it, and bulk diffusion through the metal particle to the NT edge and (ii) direct impingement of carbon into the metal particle and bulk diffusion through the particle to the NT edge.

binding energies, about 1 eV per atom,³⁴ leads to easier dissolution of C atoms if they are located in pentagons as compared with hexagons. The energy diagram given in Fig. 3 shows the energy levels for carbon atoms in vapor, metal-carbon solution (E_s) and at the NT edge: (i) at a pentagon corner (E_{bp}) or (ii) at a hexagon corner (E_{bh}).³⁴ The energy difference $\Delta H = E_s - E_b$ (dissolution heat) defines the solute concentration of carbon in equilibrium with the solid phase, i.e., $c_{\text{eq}} \propto \exp(-\Delta H/k_B T)$. Thus, given that the binding energy for a carbon atom in the pentagon is higher than for a hexagon one finds that carbon solute concentration in equilibrium with the “pentagonal phase” is higher than that in equilibrium with the “hexagonal phase.” That is, the resulting ratio of equilibrium C concentration in the metal particle relative to the “pentagonal phase” to that of the “hexagonal phase” is $\exp(E_{bp} - E_{bh}/k_B T) = \exp(1 \text{ eV}/k_B T) \approx 10^2 - 10^5$ for $T = 1000 - 2000$ K. Therefore, during growth metal particles supersaturated with carbon relative to “hexagonal phase” remain undersaturated relative to “pentagonal phase,” effectively dissolving pentagons if they form on the edge, and thereby preventing NT wall growth termination by pentagon formation and edge closure.

Our analysis shows that in feeding NT growth the C flux through the metal nanoparticle surface remains negligibly small as compared with the contribution of SD over the NT surface. Let us consider the competition of SD flux over the NT surface with that directly impinging and diffusing through the catalyst particle attached to the NT end (see Fig. 4). Let us note that C atoms are found to have large adsorption energy with the NT wall surface, $E_a \sim 1.8$ eV, and low activation energy of SD, $\delta E_a \approx 0.13$ eV.³⁴ Thus, the growth of NTs can be fed by all the C atoms adsorbed on the NT surface over SD length (the distance the adatoms may migrate over the surface prior to desorption) given by

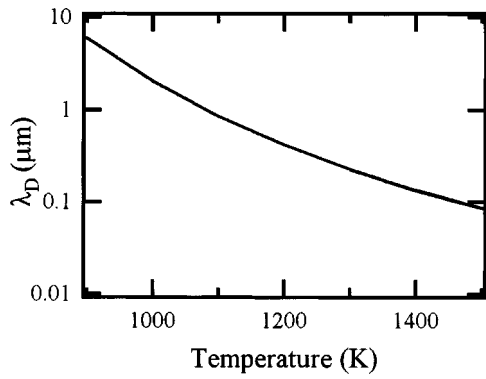


FIG. 5. Surface diffusion length of the C atom on the NT surface as a function of temperature.

$$\lambda_D \approx (D_s \tau_a)^{1/2} \approx a_0 \exp[(E_a - \delta E_D)/2k_B T], \quad (4)$$

where $\tau_a \approx \nu^{-1} \exp(E_a/k_B T)$ is the adsorption time and the SD coefficient, D_s , is given by

$$D_s \approx a_0^2 \nu \exp(-\delta E_D/k_B T), \quad (5)$$

where $\nu = (1-3) \times 10^{13}$ Hz is the thermal vibration frequency and a_0 is the intersite distance.

Figure 5 shows that for the typical temperature range of $T = 900-1200$ K the value of SD length is within $\lambda_D \approx 6.0-0.4$ microns. It should be noted that for $T = 900$ K, $\lambda_D \approx 6.0 \mu\text{m}$ exceeds the characteristic length within which species impinge into the NT surface by ballistic impingement into the NT forest (see Fig. 2) meaning that all chemically active carbon species impinging onto the NT surface are able to migrate back to the NT tip and to incorporate into the NT wall. In contrast, for higher temperatures $T > 1150$ K the diffusion length becomes shorter than $1 \mu\text{m}$ meaning that a considerable number of C species impinging into and chemisorbing on the NT surface at distances greater than this length are unable to migrate and to incorporate into the tip.

Let us now consider the carbon fluxes involved in feeding the growth of a NT rooted at a metal particle (Fig. 4) exposed to C flux from gas, $Q = P_c / (2\pi m k_B T)^{1/2}$. The total C flux onto the particle surface is $\approx Q \psi \pi R_p^2$, where R_p is the particle radius and $\psi \approx 2$ is a factor which takes into account the part of the particle surface subject to the C flux incoming from gas. The flux of C atoms into the NT surface and feeding growth by SD is $\approx Q 2\pi R L$, where L is the current length of the NT (it is assumed here that $L \ll \lambda_D$). Thus, the SD contribution becomes significant already when $L \approx R_p$, i.e., immediately after the nucleation, and prevails when $2RL \gg \psi R_p^2$, i.e., $L \gg R_p$.

The contribution of SD flux over the NT surface to feeding NT growth appears even more significant if one considers the diffusion pathways of C penetration to the growth edge through the metal particle and the related bulk diffusion times. That is, the characteristic time for bulk diffusion is defined by

$$\tau_d \approx l^2 / D_b, \quad (6)$$

where l is the characteristic path length of diffusing species and D_b is the bulk diffusion coefficient,

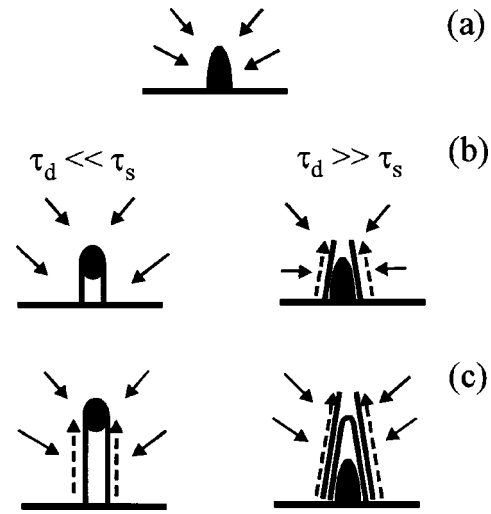


FIG. 6. Sketch of the selection mechanism of the NT growth mode depending on characteristic times of (i) diffusion through the nanoparticle and (ii) nanoparticle surface saturation with carbon.

$$D_b \approx D_0 \exp(-\delta E_b / k_B T), \quad (7)$$

where $D_0 \approx 0.1-0.5 \text{ cm}^2/\text{s}$ and $\delta E_b \approx 1.4-1.6 \text{ eV}$ for practical growth temperatures $T = 1000-1500 \text{ K}$.^{45,46}

For C atoms incoming to the particle surface via diffusion over the NT surface the bulk diffusion path length (#1 in Fig. 4) is of the order of the NT wall thickness, $\approx \delta$, and the characteristic time is $\approx \delta^2 / D_b$. In contrast, for C atoms impinging directly into the metal particle surface the bulk diffusion path length (#2 in Fig. 4) is of the order of the metal particle radius, R_p , and, therefore the characteristic time is $\approx R_p^2 / D_b$, which is $\gg \delta^2 / D_b$ whenever $R_p / \delta > 3$.

Thus, the contribution of NT surface diffusion to the flux of C atoms to the NT edge in the postnucleation stage is (i) overwhelming in comparison with the contribution of C flux impinging directly into the metal particle surface and (ii) the characteristic time for the bulk diffusion transfer of this flux through the metal particle to the NT edge, where carbon incorporation into the NT wall takes place, is significantly smaller than that corresponding to bulk diffusion pathway of C atoms impinging directly into the metal particle surface. It should be mentioned that in CVD process, depending on feed gas and conditions, the diffusing species are not necessarily restricted to isolated carbon atoms, and additionally carbon flux through the metal particle may also be decelerated by the additional step associated with thermally activated dissociation of hydrocarbons on the nanoparticle surface ongoing prior to carbon dissolution in metal.

B. Mechanism of growth mode selection

Bulk diffusion and carbon flux through metal nanoparticle plays an important role in the initial stage defining whether the nanoparticle remains at the bottom or is held on the tip of the growing NT (schematized in Fig. 6). This selection is defined by two characteristic times, dependent on D_b : (i) the diffusion time required for C penetration to the bottom of the nanoparticle from its upper surface $\tau_d \approx R_p^2 / D_b$ [Eq. (6)], and (ii) the surface saturation time, τ_s ,

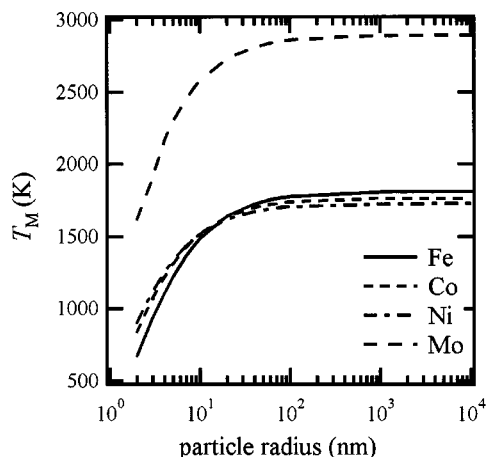


FIG. 7. Melting temperature of spherical metal nanoparticle as a function of radius.

corresponding to the increase of C concentration to the saturation level triggering C precipitation directly on the particle surface,

$$\tau_s \approx C^*{}^2 D_b / Q_c^2, \quad (8)$$

where C^* is the saturation concentration of C in the metal nanoparticle and Q_c is the carbon flux into nanoparticle. This expression comes from the solution of the diffusion equation of carbon penetration into a solid body from its surface.⁴⁸

If $\tau_d \gg \tau_s$ the surface saturates with C much faster than C penetrates to the bottom, and, therefore, C precipitates at the nanoparticle surface, which then provides a nanoscale template for NT nucleation. When $\tau_d \ll \tau_s$ C penetrates to the bottom much faster than the nanoparticle surface reaches the supersaturation threshold. In this case C segregation and precipitation starts at the bottom lifting the nanoparticle, and later on maintaining it at the NT tip.

Both expressions, i.e., Eqs. (6) and (8), include the bulk diffusion coefficient D_b , which depends on the metal used, and also on whether the metal particle remains in a solid or a liquid state during NT growth. The possibility of metal nanoparticle liquefaction at significantly lower temperatures as compared with those given by the solid–liquid phase diagrams has been suggested in several papers.^{19,49–53} Relevant carbon–metal binary phase diagrams⁵⁴ show that metal saturation with C causes a significant decrease in the melting temperature. That is, for the C–Co alloy the solidification temperature is ≈ 1593 K, for C–Ni ≈ 1600 K, and for C–Fe ≈ 1426 K.⁵⁴

An additional effect contributing to a decrease in the temperature of melting, well known in crystal growth theory as the Gibbs–Tompson effect, takes into account the dependence of the melting temperature on the particle radius,⁵⁵

$$T_M = T_{M0} \exp(-\gamma K / \Delta H), \quad (9)$$

where T_{M0} is the melting temperature of the flat surface, γ ≈ 2 J/m² is the surface tension of metals, ΔH is the latent

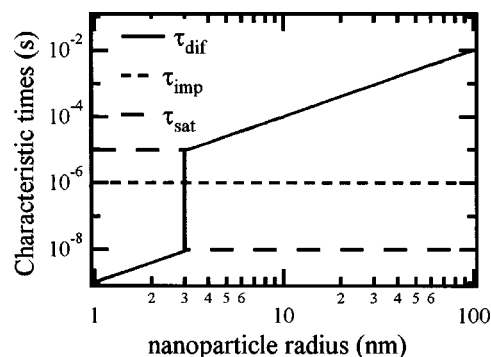


FIG. 8. Characteristic times as a function of nanoparticle radius: (a) carbon diffusion time through the nanoparticle, Eq. (6), (b) time for surface saturation with carbon, Eq. (8), and (c) carbon impingement time into nanoparticle surface, Eq. (10).

heat per volume unit, and $K = 1/\rho_1 + 1/\rho_2$ is the curvature with ρ_1 and ρ_2 as the main radii of curvature of the metal nanoparticle.

Figure 7 shows that for the pure typical metals the melting temperature decreases sharply when $R < 20$ – 30 nm and for $R < 10$ nm the fall in T_M may be several hundred Kelvin. The combination of this effect together with the above-mentioned lowering of the carbon–metal eutectic point (≈ 175 K for Co, for Ni ≈ 110 K, and for Fe ≈ 385 K) and together with other effects [such as impingement of ions in plasma enhanced CVD (Ref. 19) and also heat release of chemical reactions and NT solidification at the nanoparticle surface] may lead to the melting of metal nanoparticles even at very low substrate temperatures. A recent experimental study suggests that melting of Ni nanoparticles and change in growth mode of carbon nanotubes takes place between 700 and 800 °C.⁵¹

The value of D_b depends on the nanoparticle state and this effect is crucial for the growth selection mode defined by Eqs. (6) and (8) (see Fig. 8 where estimates of the characteristic times are given as a function of nanoparticle radius). In particular, at 1000 K an Fe nanoparticle with $R_p < 3$ nm remains liquid with $D_b \approx 10^{-5}$ cm²/s, whereas for $R_p > 3$ nm the nanoparticle is solid with $D_b \approx 10^{-8}$ cm²/s. Metals saturate at ≈ 10 – 12 at % of C (Ref. 54) and $C^* \approx 10^{22}$ cm⁻³. Hence, for typical conditions $T = 1000$ K and $P_c \approx 2600$ Pa (≈ 20 Torr) assuming $Q_c = Q = P_c / (2\pi m k_B T)^{1/2} \approx 10^{22}$ cm⁻² s⁻¹ one gets for a nanoparticle of $R_p = 10$ nm that $\tau_d \approx 10^{-4}$ s $\gg \tau_s \approx 10^{-8}$ s meaning that its surface saturates much faster than C penetrates to its base. Surface saturation isolates the nanoparticle from further C penetration leading to C precipitation, and NT nucleation and growth on the upper part of the nanoparticle. In contrast, for a liquid nanoparticle of $R_p = 1$ nm $\tau_d \approx 10^{-9}$ s $\ll \tau_s \approx 10^{-5}$ s. This implies that the NT starts to grow at the nanoparticle base because of more favorable conditions for carbon precipitation as compared with a free nanoparticle surface due to (i) interaction with the substrate surface, which provides an additional energy potential well for carbon atom precipitation and (ii) enhanced solidification heat dissipation by heat conduction into the substrate.

This mode has some additional restrictions. First, for the

particle not to be covered with carbon the characteristic diffusion time, τ_d , should also be much smaller than the characteristic impingement time,

$$\tau_{\text{imp}} \approx 1/(Q_c a_0^2), \quad (10)$$

with which C species impinge into the particle (where a_0 is the interatomic distance). Otherwise, the C concentration increases leading to C precipitation on the nanoparticle surface. For $T=1000$ K and $Q \approx 10^{22} \text{ cm}^{-2} \text{ s}^{-1}$ for Fe nanoparticle of $R_p=1$ nm $\tau_{\text{imp}} \approx 10^{-6}$ s $\gg \tau_d \approx 10^{-9}$ s, and hence, the nanoparticle remains at the NT tip and is not covered by C during growth. In contrast, for an Fe nanoparticle of $R_p=10$ nm $\tau_{\text{imp}} \approx 10^{-6}$ s $\ll \tau_d \approx 10^{-4}$ s meaning that the nanoparticle lifted on the NT tip will with time become covered by C. Second, the possibility of nanoparticle lifting depends also on whether the energy gain, resulting from C transition from the nanoparticle into the initial NT ring, is sufficiently high to overcome the interface energy between nanoparticle and substrate, $\approx \gamma R_p^2$ (γ is the interface energy per unit area).

The above analysis may produce the impression that the growth selection mechanism is mainly due to the liquid/solid transition taking place with decrease in nanoparticle radius. We would like to stress here that in estimating the carbon flux we have simplified the problem equating it here to the ballistic flux from the gas, i.e., $Q_c \approx Q = P_c/(2\pi mk_B T)^{1/2}$. Our analysis of the kinetics of solid surface saturation by carbon under the hydrocarbon flux⁴⁸ shows that a number of intermediate stages may be involved on the substrate surface. These steps are able to lead to a significant decrease in the resulting carbon flux, Q_c , into the nanoparticle as compared with the ballistic impingement rate, Q , used here. The absence of relevant microenergetics data does not allow us to provide an exact estimate for this effect. However, taking into account that these intermediate kinetics steps have activation energy barriers and, therefore, are described by the exponents,⁴⁸ one may conclude that these steps may decrease by two–three orders of magnitude the value of Q_c which should enter into Eqs. (8) and (10) instead of the ballistic approximation. This would increase the saturation time to the level where the transition threshold from one mode to another, i.e., $\tau_d \approx \tau_s$, will correspond to the solid state. In this case a strong dependence of C flux Q_c into the nanoparticle on the temperature should appear suggesting that the characteristic time for surface saturation with C may decrease with increase in T (due to the exponential behavior of Q_c on T and $\tau_s \propto Q_c^{-2}$) faster than the characteristic time of C diffusion through the particle defined by Eq. (6). This leads to the situation where, at lower temperature, the metal particles will detach from the surface whereas at larger temperatures they will remain at the substrate even in the liquid state. Such a situation has recently been observed in experiments with Ni.⁵¹

This selection mechanism for NT forest growth modes defines the final morphology of NTs and their properties. A nanoparticle remaining at the NT base provides an initial template with nanoscale curvature for NT nucleation predefining the morphology of the resulting NTs. Cylindrical nanoparticles are able to form NTs with straight walls, whereas on conical nanoparticles conical NT nuclei tend to

form leading to growth of bamboolike NTs.¹⁸ The formation of “bamboolike” structures in the CVD process may be attributed to the periodic closure and subsequent nucleation of successive conical layers (Fig. 6). Two slightly different scenarios of bamboolike growth are possible. In the first scenario the increase in the first layer length (i) provokes an increase of surface concentration which triggers next layer nucleation. The second layer, fed by SD from both sides of the growth edge (ii) has a larger growth rate, catches up with the underlying layer and inhibits its growth (iii) causing it to close up. In the second scenario the first nucleating NT layer grows until closure due to the predefined conical shape. After closure the surface sink for C is cut off, and surface concentration of C species increases and triggers the nucleation of the new layer which grows until its own closure, triggering new layer nucleation.

A nanoparticle held on the NT tip can inhibit the formation of pentagons and NT closure⁴¹ allowing the growth of straight wall NTs. Nevertheless, numerous observations show that even with the presence of a nanoparticle on the NT tip bamboolike or skeletal compartments are often formed behind the nanoparticle.^{19,56,57} One possible qualitative explanation for such bamboo or skeletal structures has recently been suggested based on thermodynamics and the surface diffusion mechanism.⁵⁶ Quantitative analysis of this mechanism reveals the onset of NT growth auto-oscillations including repeated C accumulation in the metal particle followed by precipitation. The C content in the metal nanoparticle during growth is defined by a balance between (i) carbon sink into the growing NT wall given by $\approx 2\pi R\Omega^{-1}dL/dt$ (where Ω is the area occupied by C atom in hexagonal network) and (ii) carbon flux into the upper part of the nanoparticle surface $\approx 2\pi R^2Q_c$ and (iii) carbon flux provided by SD over the NT surface, $\approx 2\pi RLQ_c$. This balance leads to the following equation for carbon concentration, C , in the metal particle:

$$Vdc/dt \approx 2\pi R^2Q_c + 2\pi RLQ_c - 2\pi R\Omega^{-1}dL/dt, \quad (11)$$

where V is the particle volume.

The contribution of the SD term increases with increase in NT length creating finally a very high carbon supersaturation at the bottom part of the nanoparticle and triggering precipitation of a new layer which triggers the formation of a new bamboo compartment and interrupts the growth of the previous layer. That is, even assuming a linear increase in the NT length with time (which may in fact be exponential as will be shown later) one finds from Eq. (11) that the contribution of the SD provides a parabolic increase of carbon content in the nanoparticle, $c \propto t^2$, as compared with the linear increase given by C flux into the nanoparticle $c \propto t$. This situation is repeated when a new compartment becomes long enough, providing a sufficiently large C flux and critical supersaturation in the nanoparticle. This mechanism of periodic supersaturation and formation of a new bamboo compartment causes an auto-oscillatory growth mode. It should be noted that critical supersaturation arises in the metal particle near the NT root because of the contribution of SD near it (if it were due to C flux from the gas the upper part should

rather be supersaturated leading to C precipitation onto the upper part of the nanoparticle fully covering it with carbon condensate).

IV. METAL PARTICLE MEDIATED TIP GROWTH KINETICS

A. Initial stage

Let us now consider in detail NT forest growth for the case when metal particles are held on NT tips. In this practically important case the metal particle may be easily removed after forest growth by chemical etching techniques. In considering this case we neglect the C flux impinging directly into the particle surface (for the validity of this simplification see Fig. 4 and related explanations in Sec. III A). We take into account only the C flux (i) impinging initially into the NT surface, (ii) diffusing over NT surface to the metal particle where the NT is rooted, and (iii) later diffusing through the particle to the NT edge. In order to reveal the interplay of SD diffusion over the NT surface and bulk diffusion through the metal particle we consider the initial NT growth stage when the NT forest length is much smaller than the ballistic penetration length and the C flux may be assumed to be constant over the NT surface. In this case, a simplified equation for NT growth, formulated originally to describe SWNT growth,⁴¹ may be used. In this paper we will use this equation to describe growth of a multilayered NT with a metal nanoparticle at the NT end shown in Fig. 4. Including the number of atomic layers in the NT wall, N , this equation is written

$$\begin{aligned} V &= dL/dt \\ &= -\frac{\Omega D_s}{N} \frac{dn}{dx} \\ &= \frac{\Omega k Q_c \tau_a \sinh(L/\lambda_D)}{N[\sinh(L/\lambda_D) + (k\lambda_D/D_s)\cosh(L/\lambda_D)]}, \end{aligned} \quad (12)$$

where Ω is the area per one C atom in the NT wall and k is the kinetic constant of atom incorporation into NT wall. This constant is given by

$$k \approx a_0 / \tau_{\text{inc}}, \quad (13)$$

where a_0 is the characteristic growth distance per one atom incorporation, and τ_{inc} is the characteristic time, required for the adatom to transfer from the lateral surface onto the NT edge and to incorporate into it. In general, τ_{inc} includes several steps. These steps may differ from each other by several orders of magnitude in which case τ_{inc} may be estimated as the largest time involved. In the case of open edged SWNT growth, $\tau_{\text{inc}} \approx \nu^{-1} \exp(\delta E_{\text{inc}}/k_B T)$ corresponds to a transition from the lateral surface to NT edge via an energy barrier, δE_{inc} , giving

$$k \approx a_0 \nu \exp(-\delta E_{\text{inc}}/k_B T). \quad (14)$$

In the case of MWNTs growing with a metal nanoparticle attached to the end, which is considered here, the slowest step is obviously defined by carbon atom diffusion from the edge of the external layer to the edge of the internal layer

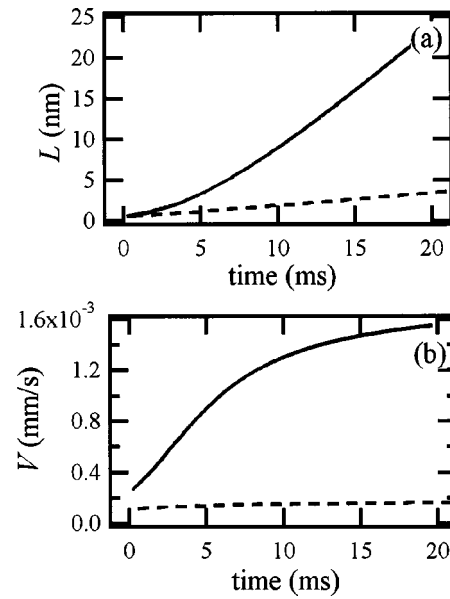


FIG. 9. Initial stage for MWNT length (a) and MWNT growth rate (b) for growth of 10 layer MWNT under control of bulk diffusion through the metal nanoparticle, $k\lambda_D/D_s \ll 1$.

through the metal layer with thickness corresponding to that of the NT wall, i.e., δ as schematically shown in Fig. 4 (we assume here that carbon diffusion at the tube–particle interface is not probable because of the deep energy well at the graphitic edges). Therefore, the time of incorporation is defined by $\tau_{\text{inc}} \approx \delta^2/D_b$ giving

$$k \approx a_0 D_b / \delta^2. \quad (15)$$

In Fig. 9 we show the analytical solution of Eq. (12),

$$L(t) + \frac{k\lambda_D^2}{2D_s} \ln \frac{\cosh(2L(t)/\lambda_D) - 1}{\cosh(2L_0/\lambda_D) - 1} = L_0 + \frac{\Omega \tau_a k Q_c t}{N} \quad (16)$$

for $T = 1300$ K and for low C flux $Q_c \approx 2 \times 10^{-19}$ $1/\text{cm}^2 \text{ s}$ (equivalent to $P_c = 10$ Pa), calculated for $E_a = 1.8$ eV and $\delta E_D = 0.13$ eV (Ref. 34) for two different modes corresponding to MWNT growth consisting of 10 atomic layers at the edge of which a metal particle is attached with diffusion coefficient corresponding to the (i) liquid metal $D_b \approx 10^{-5}$ cm^2/s (solid line), and (ii) the solid metal $D_b \approx 10^{-6}$ cm^2/s (broken line). For both cases considered in Fig. 9 the values of $\lambda_D \approx 0.2$ μm and $D_s \approx 1.9 \times 10^{-3}$ cm^2/s , and the difference in growth behavior is caused only by the kinetic constant of incorporation, Eq. (15). For the SWNT growth simulation given in a previous publication,⁴¹ at $T = 1300$ K, $k \approx 1.3 \times 10^3$ m/s, whereas for MWNT growth with a catalyst nanoparticle considered in Fig. 9, $k \approx 1.2 \times 10^{-2}$ m/s (solid line) or $k \approx 1.2 \times 10^{-3}$ m/s (broken line). Correspondingly, the growth of a MWNT with $k\lambda_D/D_s \approx 1.4 \times 10^{-2} \ll 1$ is controlled by C diffusion through the metal particle.

That is, growth of the SWNT without a metal nanoparticle and thus controlled by surface diffusion $k\lambda_D/D_s \gg 1$ is described by

$$dL/dt = \Omega Q_c \lambda_D t h(L/\lambda_D), \quad (17)$$

exhibiting exponential behavior $dL/dt \approx \Omega Q_c L$ for $L \ll \lambda_D$, and tending to a constant growth rate $dL/dt \approx \Omega Q_c \lambda_D$ for $L > \lambda_D$.

In contrast, for catalyst mediated MWNT growth shown in Fig. 9, $k\lambda_D/D_s \ll 1$. That is, the growth is controlled by diffusion through the metal particle and the growth tends to a constant value,

$$dL/dt \approx \Omega k Q_c \tau_a / N. \quad (18)$$

The initial stage of MWNT growth for the case of $D_b \approx 10^{-5}$ cm²/s shown in Fig. 9 by solid line also exhibits exponential behavior for $L < 10$ nm. An expansion of Eq. (12) into a Taylor series for $L/\lambda_D \ll 1$ gives

$$dL/dt \approx \frac{\Omega k Q_c \tau_a}{N} \frac{L/\lambda_D}{L/\lambda_D + k\lambda_D/D_s}, \quad (19)$$

which exhibits exponential growth mode $dL/dt \approx \Omega Q_c L/N$ for $L/\lambda_D \ll k\lambda_D/D_s$. Hence, for the case of $D_b \approx 10^{-5}$ cm²/s, $\lambda_D \approx 0.2$ μm, and $k\lambda_D/D_s \approx 1.4 \times 10^{-2}$ growth remains exponential as long as $L < 3$ nm and continues to depend on SD parameters as long as $L < 10$ nm. However, for a smaller value of $D_b \approx 10^{-6}$ cm²/s one has $k\lambda_D/D_s \approx 1.4 \times 10^{-3}$ and the MWNT growth is linear from the very beginning.

The growth modes depicted in Fig. 9 agree well with experimental data,³⁰ which show that the dependence of L on time may be linear or exponential depending on the metal involved in the MWNT synthesis. The presence of the exponential time dependence in MWNT growth³⁰ is a clear experimental indication of the involvement of the SD mechanism in carbon NT growth.

B. Steady-state stage and temperature dependence of the growth rate

To reveal the contribution of the SD mechanism in more detail let us consider steady state growth of the NT forest, taking into account the decay of the impinging flux along the MWNT surface and also investigating how the MWNT forest growth rate depends on the temperature. We use here a one-dimensional quasi-steady-state surface diffusion approximation,

$$D_s d^2 n/dx^2 + Q_c(x) - n/\tau_a = 0, \quad (20)$$

where n is the surface concentration and $Q_c(x)$ is the C flux distribution along the lateral surface of the NT defined by

$$Q_c(x) = Q_c \bar{F}_{\text{gas}}(x) \approx 0.5 Q_c \exp(-x/l^*), \quad (21)$$

where Q_c is the flux from a hemispherical solid angle and l^* is the characteristic decay length introduced for the analytical approximation of the angle factor distribution [Eq. (3)].

We consider here those modes where the metal nanoparticle remains at the MWNT tip using the following boundary condition on the NT edge $x=0$,

$$D_s dn/dx = kn, \quad (22)$$

where the kinetic constant k is defined by Eq. (15).

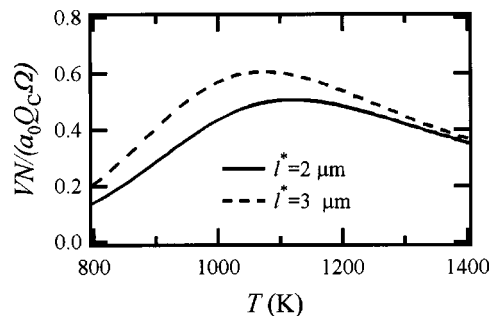


FIG. 10. Dimensionless MWNT growth rate as a function of T .

Solving Eqs. (20)–(22) and assuming that the NT length is sufficiently high, i.e., $dn/dx=0$ at $x \rightarrow \infty$ we find an equation for the MWNT forest growth rate with metal nanoparticles on the tips,

$$V = dL/dt = \frac{0.5 \Omega Q_c \tau_a k}{N(1 + \lambda_D/l^*)(1 + k\lambda_D/D_s)}. \quad (23)$$

In Fig. 10 we show the dependence of the dimensionless value of growth rate $VN/(a_0 \Omega Q_c)$ as a function of T for 10-layer MWNT growth with a metal particle at the edge and parameters for diffusion coefficient D_b , $D_0=0.1$ cm²/s and $\delta E_d=1.4$ eV, corresponding to a solid metal. The ballistic factor is estimated by Eq. (21) with typical values of $l^* \approx 2-3$ microns, which approximates well the distribution shown in Fig. 2.

These graphics show that the growth rate increases with increase in the ballistic length within which carbon flux impinges into the MWNT surface. This is caused by surface diffusion, which redirects to the NT edge carbon species adsorbing on the lateral surface.

However, the influence of this factor decays with increase in T due to $\lambda_D/l^* \ll 1$ when the increase in the ballistic length value does not increase the number of atoms which are able to reach the growth edge on the tip. Both graphics shown in Fig. 10 exhibit a maximum in the growth rate near $T \approx 1050-1100$ K which is defined by the three major effects illustrated in Figs. 11(a), 11(b), and 11(c). Figure 11(a) shows that $k\lambda_D/D_s \ll 1$ for all temperature range considered. In contrast, $\lambda_D/l^* \gg 1$ for 800–900 K and the growth rate depends on the kinetic constant of incorporation as well as on the SD and ballistic lengths as $V \approx 0.5 \Omega Q_c \tau_a k l^*/N \lambda_D$. Thus, for this mode, the growth is controlled simultaneously both by surface and bulk diffusion. For $T > 1300$ K we have $\lambda_D/l^* \ll 1$ and the growth rate is controlled solely by the kinetic constant of incorporation defined by bulk diffusion, $V \approx 0.5 \Omega Q_c \tau_a k/N$. Figure 11(b) shows a decrease in the absorption time, τ_a , with increase in T , whereas Fig. 11(c) shows an increase in k which together with the influence of the factor $1/(1 + \lambda_D/l^*)$ makes the value of V increase in the range 800–1000 K. However, when $1/(1 + \lambda_D/l^*) \rightarrow 1$ the decrease in τ_a is no longer compensated by increase in k and the growth rate ultimately decreases with increase in T .

It should be emphasized that the behavior of carbon NT forest growth as a function of T revealed by this model agrees well with experimental data.²² We are not able to

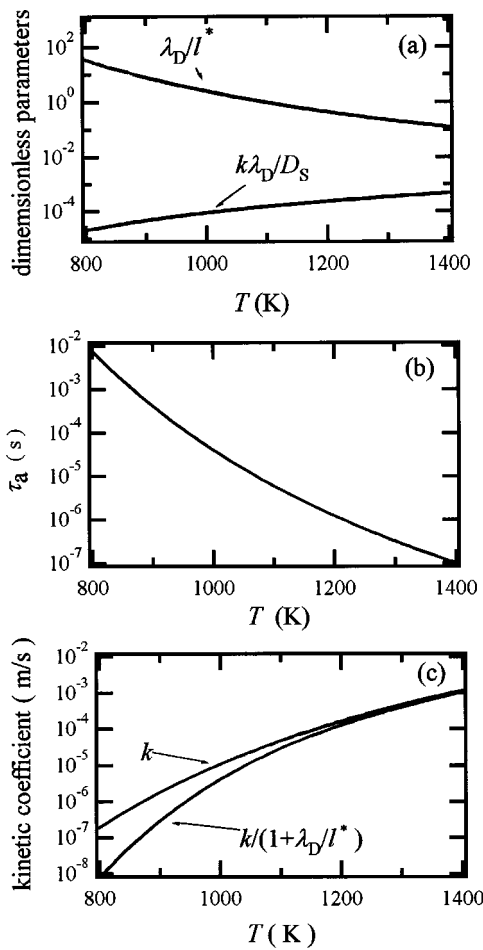


FIG. 11. Dependence of (a) dimensionless parameters, (b) adsorption time, and (c) kinetic constants.

compare absolute values of the growth rates because of the unavailability of measurements of real carbon fluxes impinging into the NT surface in the experimental study.²² Additionally, the problem contains more complicated surface chemical kinetics which should be taken into account to allow full comparison. That is, when estimating the resulting carbon flux all the thermally activated kinetics steps including carbon species desorption and dehydrogenation should be taken into account to get a proper estimate of Q_c . This would require a detailed quantum mechanical surface chemistry study. Nevertheless, even without such detail our study performed for typical solid metal diffusion parameters, i.e., $D_0 = 10^{-1}$ cm²/s and $\delta E_d = 1.4$ eV, shows the location of maximum V as function of T near 1050–1100 K which is very close to the value 1000–1050 K observed experimentally.²² Moreover, there is a good correspondence with experiment²² for the change over relative temperature intervals. That is, with an increase in T by 200 K from the maximum at $T = 1070$ K our model shows a decrease in V of about 1.5 times, whereas with a decrease in T by 200 K from the maximum our model shows a decrease in V of about 2 times. Experimental observations show more significant decreases, by 3 and 4 times, respectively.²² These discrepancies may be attributed to the incompleteness of our model in that

it neglects surface chemistry kinetics, which are also dependent on T .

V. THERMAL PHYSICS AND NT GROWTH DECELERATION EFFECT

Let us now discuss an additional effect which may influence NT forest growth. The growth rate depends on the temperature and with increase in NT length the temperature at the tip may change from that of the substrate. Such a temperature effect has been described in Ref. 58. Let us estimate here this temperature change, taking into account the specific conditions of heat transfer in the NT forest and discuss its possible implications on the growth kinetics.

The temperature distribution along an individual NT may be considered on the basis of the steady-state heat conduction approximation under the condition that the characteristic time of temperature stabilization by heat conduction, $\rho c L^2/k$, is much smaller than the characteristic time of change in NT length, $L(dL/dt)^{-1}$. For CVD growth the temperature field has enough time to adjust itself to the changing geometry. Hence, in this case the temperature distribution along an individual NT within the forest may be approximated by the steady state heat conduction equation for thermally thin shells in which heat transfer conditions are represented by equivalent energy sources and sinks as

$$k_s \frac{d^2 T}{dx^2} + \frac{1}{\delta} \{q(x) - \epsilon \sigma T^4 - h_g(T - T_g)\} = 0, \quad (24)$$

where $k_s = 250$ – 400 W/m K is the heat conductance, δ is the effective NT wall thickness (ratio of the NT wall cross section), heat transfer perimeter to $q(x)$ is the distribution of heat sources including (i) all heat effects ongoing on the NT surface and (ii) local radiative flux from surrounding surfaces (substrate, neighboring NTs), seen from a particular point x , h_g is the heat exchange with atoms of the inert gas proportional to the kinetic energy difference prior to and after the collision with the NT, $\Delta E_k \approx 3k_B(T - T_g)/2$, and to the number of collisions per unit area $Q_g = P_g / (2\pi m_g k_B T)^{1/2}$ for the buffer gas under the pressure P_g , giving⁵⁹

$$h_g \approx 3Q_g k_B / 2. \quad (25)$$

Linearization of radiation heat flux near the temperature of the substrate $\epsilon \sigma T^4 \approx \epsilon \sigma T_s^4 + 4\epsilon \sigma T_s^3(T - T_s)$ allows us to outline the influence of the heat conductance effect by using a characteristic heat conductive length defined by⁶⁰

$$l_{\text{con}} \approx \sqrt{k_s \delta / h_\Sigma}, \quad (26)$$

where $h_\Sigma \approx h_g + 4\epsilon \sigma T_s^3$ is the total heat exchange coefficient including h_g and the linear approximation of radiative heat transfer.

It should be noted that under nonuniform distribution of heat sources the temperature of the thermally thin shells remains uniform whenever the shell length $L \ll l_{\text{con}}$, due to the action of heat conduction. Temperature nonuniformity appears as soon as the shell length becomes greater than or comparable with L_{con} . In the particular case of NT forest growth, whenever the nanotube length $L \ll l_{\text{con}}$, its temperature remains uniform and is close to that of the substrate.

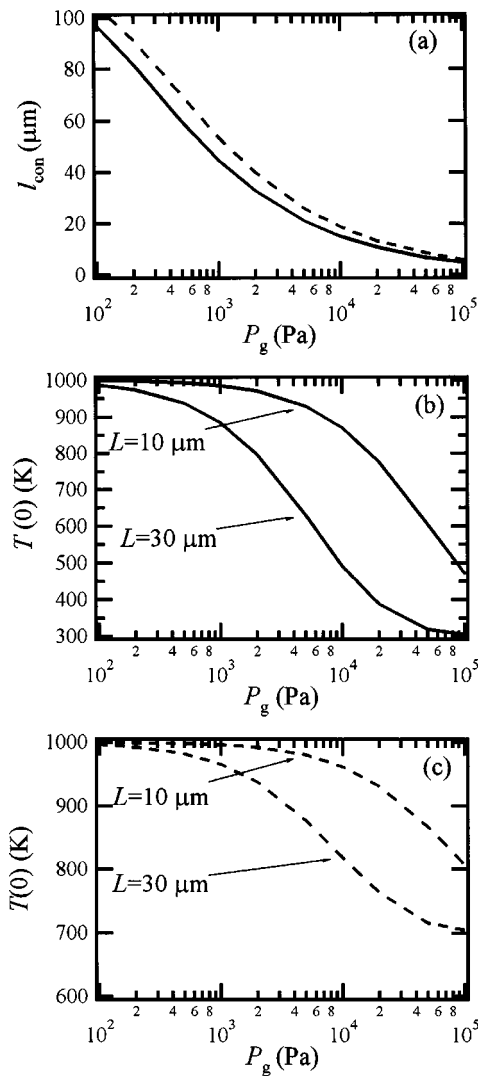


FIG. 12. Dependence of (a) heat conductive length and (b) and (c) the temperature on the tip of 10 and 30 micron long NTs (10 atomic layers) as a function of $P_g(\text{He})$ for $T_g=300\text{ K}$ and $T_g=700\text{ K}$, respectively.

Only when $L > l_{\text{con}}$ the temperature at the NT tip will differ from that of the substrate and will be defined by the heat balance with the gas, eventually tending to the temperature of gas. In particular, in Fig. 12 we show the conductive length (a) and the temperature change on the NT tip for different NT lengths L as a function of the ambient pressure for (b) $T_g=300\text{ K}$ and (c) 700 K , respectively. A solution of Eq. (24) is obtained analytically using linearization near $T_s=1000\text{ K}$. The radiative heating from the substrate and the neighboring NTs as well as from the surrounding cold wall reactor is approximated in Eq. (24) by

$$q_r(x) \approx [1 - 0.5 \exp(-x/l^*)] \epsilon \sigma T_s^4 + 0.5 \exp(-x/l^*) \epsilon \sigma T_0^4, \quad (27)$$

which is similar to the ballistic impingement function, Eq. (21), due to the formal equivalency of the ballistic impingement and radiation flux incoming from the same solid angles. The problem is solved for black body approximation with the boundary condition $T=T_s$ at the NT root ($x=L$). The second boundary condition on the NT tip ($x=0$) includes heat

release of sublimation, $-k_s dT/dx = V \Delta H$ (ΔH is the heat release at the NT edge per volume unit). However, its contribution to the temperature on the NT tips at practical growth rates of NT forests of 10 nm/s (Ref. 22) is negligibly small. The thermal effect of the nanoparticles, which dimension is much smaller than the NT length, is assumed to be negligibly small.

In particular, Fig. 12 a shows the value of l_{con} for a carbon NT consisting of 10 atomic layers for $T_s=1000\text{ K}$ and $k_s=250\text{ W/m K}$ as a function of the ambient gas pressure for $T_g=300\text{ K}$ (solid) and 700 K (broken). This figure shows that the heat conductive length decreases sharply from $l_{\text{con}} \approx 100\text{ }\mu\text{m}$ for $P_g=10^2\text{ Pa}$ to $l_{\text{con}} \approx 5\text{ }\mu\text{m}$ for $P_g=10^5\text{ Pa}$. The calculated variation of the temperature on the NT tip shown in Figs. 12(b) and 12(c) strictly follows the behavior of l_{con} . That is, when $P_g < 10^3\text{ Pa}$ for a NT with $L=10\text{ }\mu\text{m} \ll l_{\text{con}} \approx 100\text{ }\mu\text{m}$ the temperature on the tip remains close to that of the substrate $T_s=1000\text{ K}$. In contrast, when $P_g=10^5\text{ Pa}$ for NTs with $L=30\text{ }\mu\text{m} \gg l_{\text{con}} \approx 5\text{ }\mu\text{m}$ the temperature on the tip reaches that of the gas.

Figures 12(b) and 12(c) show that with an increase in the NT length the temperature may decrease leading to deceleration of NT growth. One of the reasons why we have provided the calculations for $T_g=300$ and $T_g=700\text{ K}$ is to take into account the effect of the substrate, which is able to heat up the gas, leading to the formation of a near-surface heated layer, the so-called boundary layer which may completely cover the NT forest, preserving its temperature close to T_s . The determination of the boundary layer thickness would require a simulation of a complex gas flow and heat transfer problem. In general, the boundary layer thickness is known to increase with decrease in pressure and, together with the complex geometry of NT forest, this may cause the formation of a stagnant near surface gas layer with increased temperature which should inhibit heat dissipation from the NT surface. Moreover, the ballistic mode of gas species penetration into the NT forest (see Fig. 1) suggests that only the upper part within the top 10 microns is effectively cooled by gas species (by direct collisions) whereas for the part below this range the heat dissipation efficiency decreases because of the effective increase in T_g of the gas in the intertube space. Nevertheless, the heat conductive length does not depend strongly on T and for $L \gg l_{\text{con}}$ the temperature on the NT tip will be defined by the balance with the gas (the influence of the substrate temperature through the mechanism of heat conductance becomes negligible).

Figures 12(b) and 12(c) show what the temperature on the NT tip would be if the NT had the length of 10 or 30 microns. In reality, this figure shows that the NT may not reach this length because of the temperature fall on the tip. Many experimental studies on NT forest growth report growth rate deceleration when the NT forest length attains a level well similar to the heat conductance length: growth deceleration is reported in Ref. 22; another experimental study reports that, during synthesis the growth rate started to decrease for NT forest lengths over 30 microns (after about 40 min of growth).²¹ The authors suggest that with increase in NT forest length, the rate of carbon penetration decelerates, leading to decrease in NT growth rate. Our model sug-

gests that it is caused by the temperature decrease on the upper part of the NTs where we believe growth takes due to the lack of chemically active carbon penetration to the bottom of the forest several dozen microns in depth. A similar effect was recently observed and interpreted as a time dependence anomaly.²⁷ Some papers^{3,6} report the possibility of NT forest growth by CVD from acetylene up to 2 mm in height, showing that this growth limitation may be avoided.

Our estimates given in Fig. 12 suggest that the higher the pressure the smaller the length of the NT forest which may be grown. In particular, our estimates show that for $P_g = 10^5$ Pa the maximal length of NT forest will be several microns and after that NT growth in the axial direction should stop because the NT tip will be “frozen,” disabling the growth process. However, for NT forest dimensions of several microns carbon deposition may actually continue, leading to NT radial extension at the bases, where the temperature is kept close to T_s . This result of our model agrees well with the experimental results of Ago *et al.*¹⁶ on NT forest growth performed at atmospheric pressure. Analysis of the temperature dependence of Eq. (20) suggests that the atoms adsorbing on the tips held at lower temperature may provide higher concentration of the adsorbate leading to C diffusion towards the NT base. An additional contribution of adsorbate flux towards the NT bases may also be provided by the temperature gradient along the NT. This arises from consideration of the full expression for SD flux written via the chemical potential of the adsorbate, μ , which includes an entropy related term depending on T , i.e., $k_B T \ln(n/n_0)$ (n_0 is surface density of the adsorption sites). This flux, written as⁵⁵

$$J_s = - \frac{nD_s}{k_B T} \text{grad } \mu$$

$$= -D_s \text{grad } n + nD_s \ln(n/n_0) T^{-1} \text{grad } T, \quad (28)$$

should formally enter into the related SD equation, $-\nabla J_s + Q_c - n/\tau_a = 0$, to account properly for its effect on NT growth kinetics. A contribution of this effect to the growth kinetics may be expected for cases when the SD length scale, λ_D [Eq. (4)], is close to that of the heat conductance length, l_{con} [Eq. (26)]. For cases when $l_{\text{con}} \gg \lambda_D$ the growth kinetic effects may be estimated based on the simplified form of the SD equation [Eq. (20)] taken at the temperature of the NT tip. For $L \ll l_{\text{con}}$ the temperature of the NT may be assumed uniform and the SD approximation (20) may be used, independently of the relationship between λ_D and l_{con} .

Even a moderate temperature change on the NT tip is able to decrease significantly the diffusion time through the nanoparticle body, leading to the precipitation of carbon on the upper part of the metal nanoparticle and a change of growth mode or NT growth termination. For instance, precipitation of carbon on the metal particle surface can change the NT growth mode to the homoepitaxial nucleation and growth of a new compartment at the upper part of the NT resulting in the entrapment of the metal particle within the NT body observed experimentally (for instance, see Ref. 61).

VI. SUMMARY AND CONCLUSIONS

In conclusion let us summarize the main results:

(i) For typical conditions of CVD growth the mean free path of C species in gas is much larger than the typical distance between the NTs. Due to this effect, the chemically active carbon species are unable to penetrate to the bottom of a several dozen micron deep NT forest. Rather, the majority of them collide with the NT surface, chemisorbing within a few microns of the NT forest top, and diffuse over the NT surface feeding growth at the NT tips. For typical parameters the ballistic rate at which species impinge into the NT surface decays quasiexponentially, i.e., $\propto \exp(-x/l^*)$, from the top to the bottom with a characteristic decay length of $l^* \approx 2-3$ microns. Thus, wherever metal nanoparticles remain during the growth, i.e., on the NT tip or on the substrate, growth takes place on the NT tip when NT length becomes much larger than this characteristic decay length. In particular, this explains why in growth experiments with metal nanoparticles remaining at the substrate the upper part of NTs, which are subject to significantly larger C fluxes, remain free of any kind of C deposit, i.e., graphite or amorphous carbon, which are well known to appear in C film growth in plasma assisted CVD using CH_4 or C_2H_2 with low H_2 content. In contrast, by assuming that the growth occurs at the upper tips and chemically active carbon species do not penetrate to the forest bottom, one can understand why the bottom part of the NT forest remains unfilled by any kind of carbon deposit, and why the bottom part of NTs do not fatten with time.

(ii) C dissolution and bulk diffusion through the catalyst nanoparticle plays a major role in selection of NT nucleation and growth mode, defining on the one hand the characteristic diffusion time of C to the nanoparticle bottom, τ_d , and, on the other hand, the characteristic time for nanoparticle surface saturation by C, τ_s . The competition of these processes is suggested to define whether the metal particle remains at the substrate, or is lifted and held at the NT tip during the growth. If $\tau_s \gg \tau_d$ C precipitation and NT growth starts at the particle bottom, at the interface with the substrate, lifting the metal particle to the NT tip and allowing growth of NTs with straight walls. In contrast, if $\tau_s \ll \tau_d$, C precipitates on the upper part of the particle, which serves as NT nucleation site with nanoscale curvature. After nucleation, the metal particle remains at the substrate, isolated from the impinging C flux, and does not participate further in the growth process. In this case the mechanism of SD, coupled with the mechanism of homoepitaxial nucleation of new layers, provides repeated growth inhibition, closure of the underlying layers, and new layer nucleation and growth, leading to the eventual formation of the observed bamboolike structures.

(iii) The parametric analysis of the surface diffusion model of NT growth also includes a kinetic constant of incorporation which takes into account the diffusion coefficient of carbon through the metal particle. This analysis shows that due to particle NT growth shifts from surface diffusion control to control by bulk diffusion through the particle. The model shows a variety of possible growth modes, from linear to exponential NT growth versus time, agreeing well with reported experimental data. Even in the cases when NT

growth is limited by diffusion through the nanoparticle the initial stage may be controlled by the SD flux. This mode is characterized by the exponential behavior, when the growth rate is proportional to NT length, i.e., to the ballistic flux impinging into the NT surface and channeled to the NT edge by surface diffusion.

(iv) Thus, the presence of an exponential NT growth stage is a clear experimental indication of the involvement of surface diffusion in NT growth.

(v) Under the specific conditions of MWNT forest growth, i.e., the characteristic decay length of the ballistic flux has the same order of magnitude as the SD length, the growth rate is shown to be under simultaneous control of surface diffusion and diffusion through the metal nanoparticle. A parametric study performed for typical parameters of bulk diffusion in metals reveals the existence of a in growth rate maximum near 1050–1100 K, observed experimentally for NT growth with a Ni catalyst at ≈ 1000 K.

(vi) Thermal analysis based on the heat conductance equation and characteristic heat conductance length shows that with increase in NT length the temperature on the NT tip decreases. When the NT length is much smaller than the characteristic heat conductance length the temperature on the NT tips remains close to that of the substrate. In contrast, when the NT length becomes much larger than the heat conductance length the temperature on the NT tip is defined by the heat balance with the gas and the temperature of the NT tip tends to that of the gas. We suggest that this effect explains the deceleration of NT forest growth with time reported by several experimental studies. Our analysis shows that the heat conductance length depends on the vapor pressure defining the rate of heat dissipation from the NT surface. The larger the pressure the smaller the heat conductance length. In particular, for atmospheric pressure 10^5 Pa the heat conductance length is several microns. This means that the tips of NTs of several microns should be “frozen,” disabling further NT growth, and leading to carbon condensation around the NT base where the temperature remains high. In contrast, for low pressures of $\approx 10^3$ Pa the heat conductance length is of several dozens of microns, allowing the growth of an NT forest of several dozen of microns without growth termination.

The proposed model does not take into account many microenergetic parameters, which define chemical kinetics transformation of hydrocarbon species on the surface of the NT and on the metal nanoparticle. These parameters including chemisorption of different carbon species on the surface of the NT and metal nanoparticle, and activation energies of dehydrogenation, are not available, preventing a more comprehensive analysis. Determination of these surface chemistry parameters would allow a significantly deeper insight into this subject. The determination of such parameters will also significantly increase the predictive value of this phenomenological model which even in its present simplified form generally agrees with experimental observations and allows clear interpretation of many effects.

ACKNOWLEDGMENTS

The authors would like to thank Dr. J. Hester (Australian Nuclear Science and Technology Organization) for critical reading of the manuscript and valuable comments. We would also like to thank Professor L. Chadderton (Australian National University, Australia) and Professor O. Stéphan (Univerisite Paris-Sud, France) for stimulating discussions about metal particle mediated bamboolike structure formation. O.A.L. would like to thank The National Institute for Materials Science for the continued financial support of his work via The Center of Excellence Project.

- ¹W. Z. Li, S. S. Xie, L. X. Qian, B. H. Chang, B. S. Zou, W. Y. Zhou, R. A. Zhao, and G. Wang, *Science* **274**, 1701 (1996).
- ²M. Terrones, N. Grobert, J. Olivares *et al.*, *Nature (London)* **388**, 52 (1997).
- ³Z. W. Pan, S. S. Xie, B. H. Chang, C. Y. Wang, L. Lu, W. Liu, W. Y. Zhou, W. Z. Li, and L. X. Qian, *Nature (London)* **394**, 631 (1998).
- ⁴Z. F. Ren, Z. P. Huang, J. W. Xu, J. H. Wang, P. Bush, M. P. Siegal, and P. N. Provencio, *Science* **282**, 1105 (1998).
- ⁵Z. P. Huang, J. W. Xu, Z. F. Ren, J. H. Wang, P. M. Siegal, and P. N. Provencio, *Appl. Phys. Lett.* **73**, 3845 (1998).
- ⁶Z. W. Pan, S. S. Xie, B. H. Chang, L. F. Sun, W. Y. Zhou, and G. Wang, *Chem. Phys. Lett.* **299**, 97 (1999).
- ⁷S. Fan, M. G. Chapline, N. R. Franklin, T. W. Tomblor, A. M. Cassell, and H. Dai, *Science* **283**, 512 (1999).
- ⁸J. S. Suh and J. S. Lee, *Appl. Phys. Lett.* **75**, 2047 (1999).
- ⁹S. B. Sinnott, R. Andrews, D. Qian, A. M. Rao, Z. Mao, E. C. Dickey, and F. Derbyshire, *Chem. Phys. Lett.* **315**, 25 (1999).
- ¹⁰Z. F. Ren, Z. P. Huang, D. Z. Wang, J. G. Wen, J. W. Xu, J. H. Wang, L. E. Calvet, J. Chen, J. F. Klemic, and M. A. Reed, *Appl. Phys. Lett.* **75**, 1086 (1999).
- ¹¹S. Huang, L. Dai, and A. W. H. Mau, *J. Mater. Chem.* **9**, 1221 (1999).
- ¹²C. Bower, W. Zhu, S. Jin, and O. Zhou, *Appl. Phys. Lett.* **77**, 830 (2000).
- ¹³W.-Q. Han, P. Kohler-Redlich, T. Seeger *et al.*, *Appl. Phys. Lett.* **77**, 1807 (2000).
- ¹⁴N. Grobert, M. Terrones, S. Trasobares, *et al.*, *Appl. Phys. A: Mater. Sci. Process.* **70**, 175 (2000).
- ¹⁵V. I. Merkulov, D. H. Lowndes, Y. Y. Wei, G. Eres, and E. Voelkl, *Appl. Phys. Lett.* **76**, 3555 (2000).
- ¹⁶H. Ago, T. Komatsu, S. Ohshima, Y. Kuriki, and M. Yumura, *Appl. Phys. Lett.* **77**, 79 (2000).
- ¹⁷C. J. Lee and J. Park, *Appl. Phys. Lett.* **77**, 3397 (2000).
- ¹⁸H. Cui, O. Zhou, and B. R. Stoner, *J. Appl. Phys.* **88**, 6072 (2000).
- ¹⁹M. Okai, T. Muneyoshi, T. Yaguchi, and S. Sasaki, *Appl. Phys. Lett.* **77**, 3468 (2000).
- ²⁰Y. Y. Wei, G. Eres, V. I. Merkulov, and D. H. Lowndes, *Appl. Phys. Lett.* **78**, 1394 (2001).
- ²¹C. J. Lee, S. C. Lyu, Y. R. Cho, J. H. Lee, and K. I. Cho, *Chem. Phys. Lett.* **341**, 245 (2001).
- ²²M. Chhowalla, K. B. K. Teo, C. Ducati, N. L. Rupensinghe, G. A. J. Amaratunga, A. C. Ferrari, D. Roy, J. Robertson, and W. I. Milne, *J. Appl. Phys.* **90**, 5308 (2001).
- ²³C. K. Lee and J. Park, *J. Phys. Chem. B* **105**, 2365 (2001).
- ²⁴Y. Avigal and R. Kalish, *Appl. Phys. Lett.* **78**, 2291 (2001).
- ²⁵J. I. Sohn, C.-J. Choi, S. Lee, and T.-Y. Seong, *Appl. Phys. Lett.* **78**, 3130 (2001).
- ²⁶K. B. K. Teo, M. Chhowalla, G. A. J. Amaratunga, W. I. Milne, G. Pirio, P. Lagagneux, F. Wycisk, J. Olivier, and D. Pribat, *J. Vac. Sci. Technol. B* **20**, 116 (2002).
- ²⁷B. H. J. Jeong, Y. M. Shin, S. Y. Jeong *et al.*, *Chem. Vap. Deposition* **8**, 11 (2001).
- ²⁸A. N. Obraztsov, I. Pavlovsky, A. P. Volkov, E. Obraztsova, A. L. Chuvilin, and V. L. Kuznetsov, *J. Vac. Sci. Technol. B* **18**, 1059 (2001).
- ²⁹A. Oberline, M. Endo, and T. Koyama, *J. Cryst. Growth* **32**, 335 (1976).
- ³⁰R. T. K. Baker and P. S. Harris, in *Chemistry and Physics of Carbon*, edited by P. L. Walker, Jr. and P. A. Thrower (Dekker, New York, 1978), pp. 83–161, and references therein.
- ³¹G. G. Tibbetts, *J. Cryst. Growth* **66**, 632 (1984).
- ³²O. A. Louchev, Y. Sato, and H. Kanda, *Appl. Phys. Lett.* **80**, 2752 (2002).
- ³³O. A. Louchev, *Appl. Phys. Lett.* **71**, 3522 (1997).

- ³⁴Y. H. Lee, S. G. Kim, and D. Tománek, *Phys. Rev. Lett.* **78**, 2393 (1997).
- ³⁵O. A. Louchev and Y. Sato, *Appl. Phys. Lett.* **74**, 194 (1999).
- ³⁶L. Chadderson and Y. Chen, *Phys. Lett. A* **263**, 401 (1999).
- ³⁷N. Kitamura and A. Oshiyama, *J. Phys. Soc. Jpn.* **70**, 1995 (2001).
- ³⁸O. A. Louchev, Y. Sato, and H. Kanda, *J. Appl. Phys.* **89**, 3438 (2001).
- ³⁹O. A. Louchev, *J. Cryst. Growth* **237–239**, 65 (2002).
- ⁴⁰O. A. Louchev, Y. Sato, and H. Kanda, *J. Appl. Phys.* **91**, 10074 (2002).
- ⁴¹O. A. Louchev, Y. Sato, and H. Kanda, *Phys. Rev. E* **66**, 011601 (2002).
- ⁴²This estimate comes out from the integral inequivalence of the ballistic flux impinging into the lateral NT surface, i.e., $2\pi R \int_0^L 0.5Q \exp(-x/l^*)dx$, and the flux incoming from the gas into the NT forest per specific area corresponding to one NT, is $Q(S - \pi R^2)$ under the assumption that NT length L is much larger than intertube distance $l_{\text{int}} \approx S^{-1/2}$, and $S \gg \pi R^2$.
- ⁴³W. L. Hsu, *Appl. Phys. Lett.* **59**, 1427 (1991).
- ⁴⁴W. L. Hsu, *J. Appl. Phys.* **72**, 3102 (1992).
- ⁴⁵*Physical Properties*, edited by I. S. Grigoriev and E. Z. Meilikhov (Moscow, Energoatomizdat, 1991) (*Fizicheskie Vellichini*, in Russian).
- ⁴⁶H. M. Strong and R. E. Hanneman, *J. Chem. Phys.* **46**, 3668 (1966).
- ⁴⁷J. Hester and O. A. Louchev, *Appl. Phys. Lett.* **80**, 2580 (2002).
- ⁴⁸O. A. Louchev, C. Dussarat, and Y. Sato, *J. Appl. Phys.* **86**, 1736 (1999).
- ⁴⁹E. F. Kukovitsky, S. G. L'vov, and N. A. Sainov, *Mol. Mater.* **10**, 165 (1998).
- ⁵⁰E. F. Kukovitsky, S. G. L'vov, and N. A. Sainov, *Chem. Phys. Lett.* **317**, 65 (2000).
- ⁵¹E. F. Kukovitsky, S. G. L'vov, N. A. Sainov, V. A. Shustov, and L. A. Chernozatonskii, *Chem. Phys. Lett.* **355**, 65 (2000).
- ⁵²A. Gorbunov, O. Jost, W. Pompe, and A. Graff, *Carbon* **40**, 113 (2002).
- ⁵³A. Gorbunov, O. Jost, W. Pompe, and A. Graff, *Appl. Surf. Sci.* **197–198**, 464 (2002).
- ⁵⁴*Binary Alloy Phase Diagrams*, edited by T. B. Massalski, 2nd ed. (ASM International, New York, 1992), Vol. 1.
- ⁵⁵A. A. Chernov, in *Modern Crystallography* (Springer, Berlin, 1984), Vol. III, and references therein.
- ⁵⁶L. T. Chadderton and Y. Chen, *J. Cryst. Growth* **240**, 164 (2002).
- ⁵⁷S. Trasobares, O. Stephan, C. Colliex, W. K. Hsu, H. W. Kroto, and D. R. M. Walton, *J. Chem. Phys.* **116**, 8966 (2002).
- ⁵⁸T. Laude, Ph.D. thesis, University of Tsukuba and Ecole Centrale Paris, March 2001; T. Laude and Y. Matsui (unpublished).
- ⁵⁹We assume here that the thermal accommodation coefficient is close to 1.
- ⁶⁰I. V. Baum and O. A. Louchev, *Int. J. Heat Mass Transf.* **35**, 2580 (1992).
- ⁶¹L. Yuan, K. Saito, W. Hu, and Z. Chen, *Chem. Phys. Lett.* **346**, 23 (2001).